ACS NANO
Cite This: ACS Nano 2017, 11, 12519–12525
www.acsnano.org

ARTICLE

Atomic-Scale Origin of the Quasi-One-Dimensional Metallic Conductivity in Strontium Niobates with Perovskite-Related Layered Structures

Chunlin Chen,[*,†,‡] Deqiang Yin,[‡,§] Kazutoshi Inoue,[‡] Frank Lichtenberg,[∥] Xiuliang Ma,[*,†] Yuichi Ikuhara,[*,‡,⊥,#] and Johannes Georg Bednorz[▽]

[†]Shenyang National Laboratory for Materials Science, Institute of Metal Research, Chinese Academy of Sciences, Shenyang 110016, China
[‡]Advanced Institute for Materials Research, Tohoku University, 2-1-1 Katahira, Aoba-ku, Sendai 980-8577, Japan
[§]College of Aerospace Engineering, Chongqing University, Chongqing 400044, China
[∥]Department of Materials, ETH Zürich, Zürich CH-8093, Switzerland
[⊥]Institute of Engineering Innovation, The University of Tokyo, 2-11-16 Yayoi, Bunkyo-ku, Tokyo 113-8656, Japan
[#]Nanostructures Research Laboratory, Japan Fine Ceramics Center, 2-4-1 Mutsuno, Atsuta, Nagoya 456-8587, Japan
[▽]IBM Research Division, Zürich Research Laboratory, Rüschlikon CH-8803, Switzerland

Supporting Information

ABSTRACT: The quasi-one-dimensional (1D) metallic conductivity of the perovskite-related $Sr_nNb_nO_{3n+2}$ compounds is of continuing fundamental physical interest as well as being important for developing advanced electronic devices. The $Sr_nNb_nO_{3n+2}$ compounds can be derived by introducing additional oxygen into the $SrNbO_3$ perovskite. However, the physical origin for the transition of electrical properties from the three-dimensional (3D) isotropic conductivity in $SrNbO_3$ to the quasi-1D metallic conductivity in $Sr_nNb_nO_{3n+2}$ requires more in-depth clarification. Here we combine advanced transmission electron microscopy with atomistic first-principles calculations to unambiguously determine the atomic and electronic structures of the $Sr_nNb_nO_{3n+2}$ compounds and reveal the underlying mechanism for their quasi-1D metallic conductivity. We demonstrate that the local electrical conductivity in the $Sr_nNb_nO_{3n+2}$ compounds directly depends on the configuration of the NbO_6 octahedra in local regions. These findings will shed light on the realization of two-dimensional (2D) electrical conductivity from a bulk material, namely by segmenting a 3D conductor into a stack of 2D conducting thin layers.

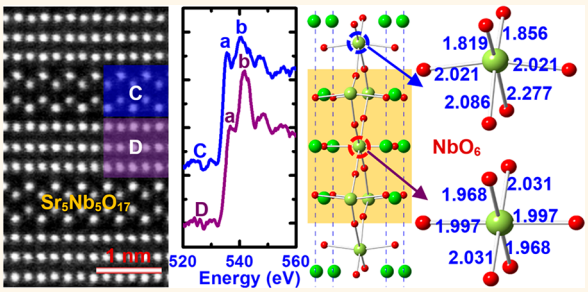

KEYWORDS: *quasi-one-dimensional metallic conductivity, layered material, ceramics, transmission electron microscopy, first-principles calculations*

Two-dimensional (2D) electrical conductivity in oxides has attracted great attention in recent years because it is of not only fundamental physical interest for studying electronic reconstruction and transport in confined regions but also of technological significance for developing advanced electronic devices.[1,2] As the most prominent example, a 2D electron gas was first discovered at the heterointerface between two perovskite insulators $SrTiO_3$ and $LaAlO_3$, and its formation origin was attributed mainly to the electronic reconstruction due to the interfacial polarity discontinuity.[3−5] Encouraged by this fascinating discovery, fabricating oxide heterostructures with 2D electrical conductivity becomes the subject of intensive research. In general, a common scientific thought among the various approaches to realize 2D electrical conductivity is creating a 2D conducting layer through fabricating a metallic heterointerface between two insulators *via* interfacial engineering technique or chemically doping a thin layer of a conducting phase inside an insulator.[6,7]

Received: September 18, 2017
Accepted: November 27, 2017
Published: November 27, 2017

DOI: 10.1021/acsnano.7b06619
ACS Nano 2017, 11, 12519–12525

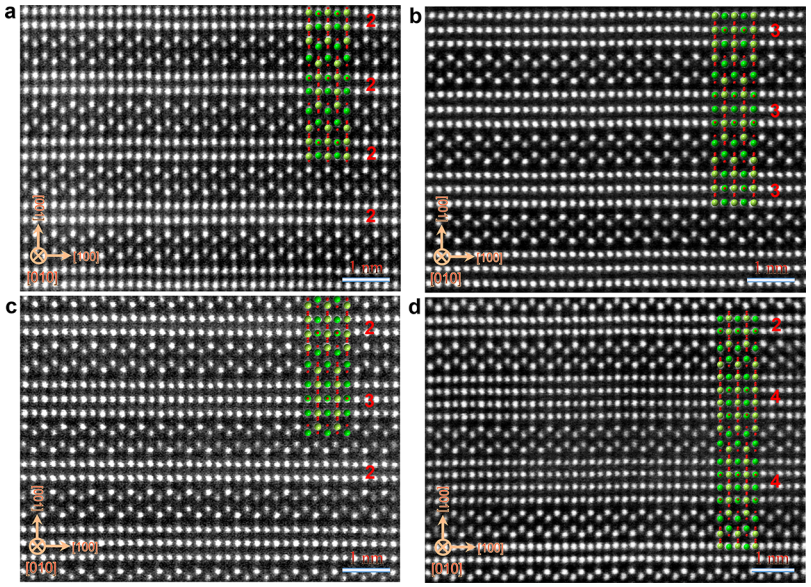

Figure 1. HAADF images showing the atomic structures of the $Sr_nNb_nO_{3n+2}$ compounds viewing from the [010] zone axis. All of the compounds have a layered structure comprising the distinct chain-like and zigzag slabs alternately stacked along the [001] direction. (a) The 2−2−2−2 type structure, corresponding to $Sr_nNb_nO_{3n+2}$ with n = 4, has uniform chain-like slabs with thickness of two atomic layers. (b) The 3−3−3−3 type structure, corresponding to $Sr_nNb_nO_{3n+2}$ with n = 5, has uniform three-layer thick chain-like slabs. (c) The 2−3−2−3 type structure, corresponding to $Sr_nNb_nO_{3n+2}$ with n = 4.5, has alternately arranged two-layer and three-layer thick chain-like slabs. (d) The 2−4−4−2 type structure, corresponding to $Sr_nNb_nO_{3n+2}$ with n = 4, 6, 6, 4, has two-layer and four-layer thick chain-like slabs. The atomic models of the $Sr_nNb_nO_{3n+2}$ compounds are overlaid on to the HAADF images. The Sr, Nb, and O atoms are represented by the green, yellow, and red colors, respectively.

On the contrary, a reverse thinking to realize the 2D electrical conductivity, which is very enlightening but has never been proposed as a guiding thought and confirmed, is segmenting a 3D conductor into a stack of 2D conducting thin layers by inserting insulating layers in between them (see Supplementary Figure S1). This idea appears to be feasible if we carefully compare the electrical properties and crystal structures between the perovskite ABO_3 and the perovskite-related $A_nB_nO_{3n+2}$ compounds.[8,9] Here we take the family of strontium niobate compounds as an example to clarify this point. As we know, $SrNbO_3$ has a perovskite structure comprising a 3D network of corner-sharing NbO_6 octahedra and exhibits a 3D isotropic electrical conductivity.[10,11] The compounds of the series $Sr_nNb_nO_{3n+2}$ have a perovskite-related layered crystal structure which can be derived by intercalating additional oxygen atoms in between the NbO_6 octahedra in $SrNbO_3$ along {110} planes.[8,9] The main building blocks of the orthorhombic $Sr_nNb_nO_{3n+2} = SrNbO_x$ structures are the NbO_6 octahedral slabs stacked along the c axis, and their thickness can be tuned by the oxygen content x. The slabs are n NbO_6 octahedra thick along the c axis. Therefore, structurally the series $Sr_nNb_nO_{3n+2}$ can be considered as the result of segmenting $SrNbO_3$ by creating layers *via* an insertion of additional oxygen.

The electrical properties of the $Sr_nNb_nO_{3n+2}$ compounds exhibit a significant change when the thickness of the NbO_6 octahedral slabs is reduced from five (n = 5) to four (n = 4) layers. The n = 5 type compound $Sr_5Nb_5O_{17} = SrNbO_{3.4}$ ($Nb^{4.8+}/4d^{0.2}$) is a highly anisotropic conductor and a quasi-1D metal with metallic behavior along the a axis,[8,9,12−17] whose dc resistivity *versus* temperature along the three crystal axes was shown in Figure 19 of ref 8 and Figure 1 of ref 12. The predominant contribution to its metallic character and density of states at the Fermi level comes from 4d electrons of those Nb ions which are located in the NbO_6 octahedra at the center of the five NbO_6 octahedra thick layers.[9,12−14] The n = 4 type compound $Sr_4Nb_4O_{14} = SrNbO_{3.5}$ ($Nb^{5+}/4d^0$) exhibits an insulating nature because its niobium valence 5+ implies zero 4d electrons per Nb ion.[8,9,18,19] (On the contrary, the niobium valence 4+ implies one 4d electron per Nb ion, rendering the $SrNbO_3$ compound conducting.)[8,11] Another compound of the series $Sr_nNb_nO_{3n+2} = SrNbO_x$ is the n = 4.5 type $SrNbO_{3.45}$ ($Nb^{4.9+}/4d^{0.1}$) which comprises an alternating sequence of five and four NbO_6 octahedra thick layers along the c axis.[8,9,13,14,20] $SrNbO_{3.45}$ is a highly anisotropic conductor and a quasi-1D metal with metallic behavior along the a axis.[8,9,13,14,20]

To reveal the atomic-scale origin of the quasi-1D metallic conductivity in the $Sr_nNb_nO_{3n+2}$ compounds and investigate the feasibility of segmenting a 3D conductor for the fabrication of 2D conducting materials, we systematically investigated the atomic and electronic structures of the $Sr_nNb_nO_{3n+2}$ compounds by combining advanced transmission electron microscopy (TEM) with first-principles calculations. We demonstrate that the electrical properties of the strontium niobates depend directly on the configuration of their NbO_6 octahedra, giving rise to a transition from 3D conductivity to 2D conductivity.

RESULTS AND DISCUSSION

The $Sr_nNb_nO_{3n+2}$ compounds $SrNbO_{3.4}$ (n = 5), $SrNbO_{3.45}$ (n = 4.5), and $SrNbO_{3.5}$ (n = 4) in crystalline form were grown by the floating zone melting method.[8,9,20] The atomic-scale structure of these compounds is shown in Figure 1 by the high-angle annular-dark-field (HAADF) STEM images along the [010] zone axis. As one can see, all of the $Sr_nNb_nO_{3n+2}$ compounds have a layered structure which comprises two distinct slabs alternately stacked along the [001] direction: One has several atomic layers linked in a straight chain-like manner, and the other appears zigzag-like. The obvious distinction

DOI: 10.1021/acsnano.7b06619
ACS Nano 2017, 11, 12519−12525

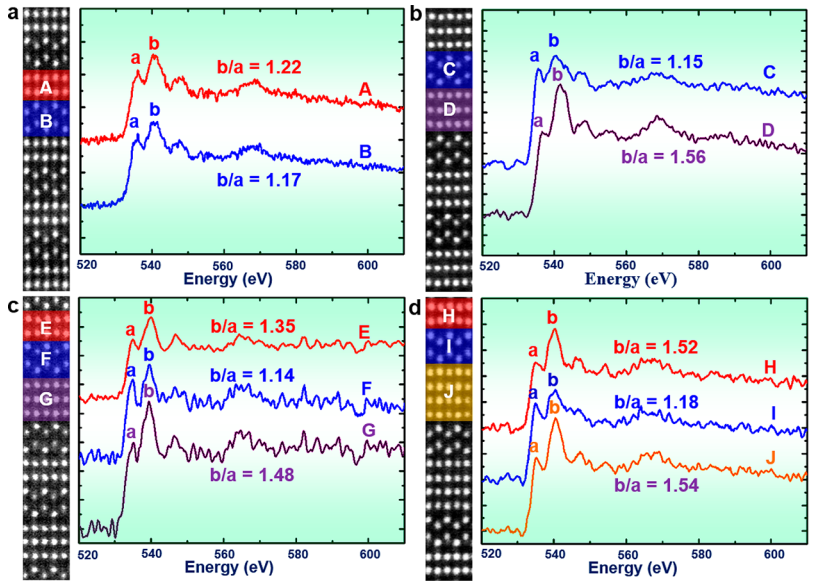

Figure 2. EELS spectra showing the O−K edges taken from the chain-like and the zigzag-like slabs of the $Sr_nNb_nO_{3n+2}$ compounds. (a) 2−2−2−2, (b) 3−3−3−3, (c) 2−3−2−3, and (d) 2−4−4−2. The O−K edges are characterized mainly by two edge onsets (denoted *a* and *b* peaks). The height ratio *b*/*a* reflects the valence state of Nb and the electrical properties of corresponding local structures. The EELS results reveal a 2D conducting nature in the 2−3−2−3, 3−3−3−3, and 2−4−4−2 type structures and a 3D insulting nature in the 2−2−2−2 type structure. The measurement error of the *b*/*a* ratios is 0.08.

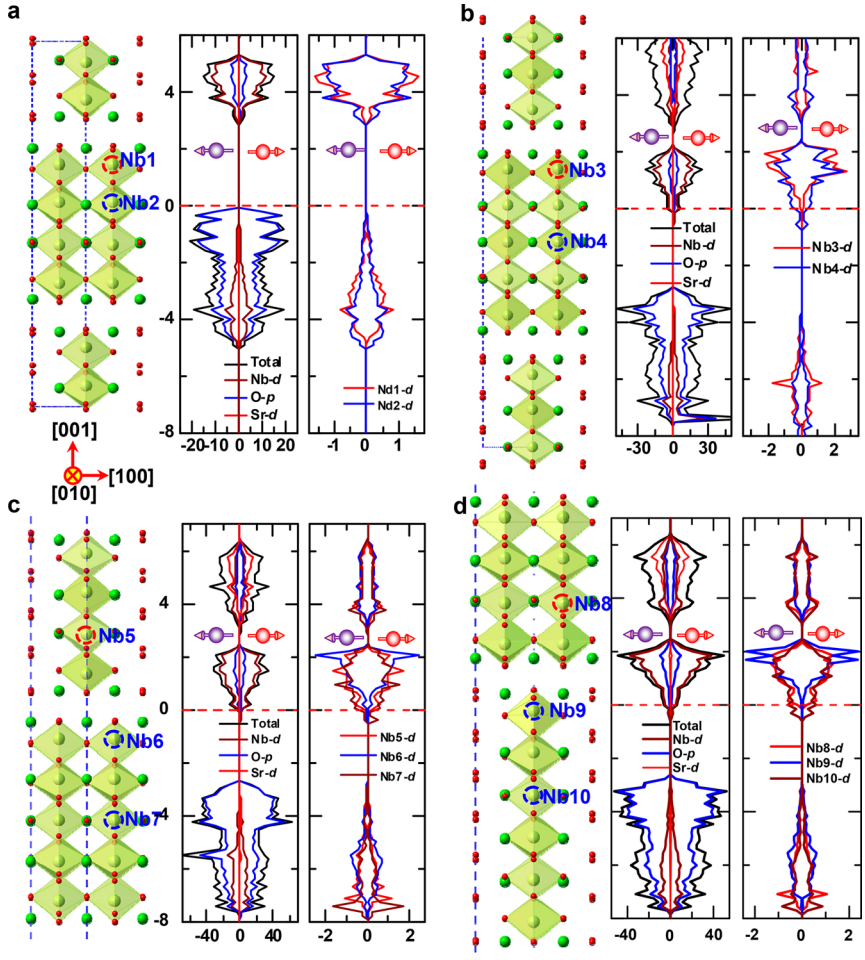

Figure 3. Optimized structural models, TDOS, and layer-resolved projected Nb-4d density of states of the $Sr_nNb_nO_{3n+2}$ compounds. (a) 2−2−2−2, (b) 3−3−3−3, (c) 2−3−2−3, and (d) 2−4−4−2. The DOS results reveal that the 3−3−3−3, 2−3−2−3, and 2−4−4−2 type structures are 2D conductors, and the 2−2−2−2 structure is a 3D insulator. The E_F is set to zero and represented by dashed lines.

DOI: 10.1021/acsnano.7b06619
ACS Nano 2017, 11, 12519−12525

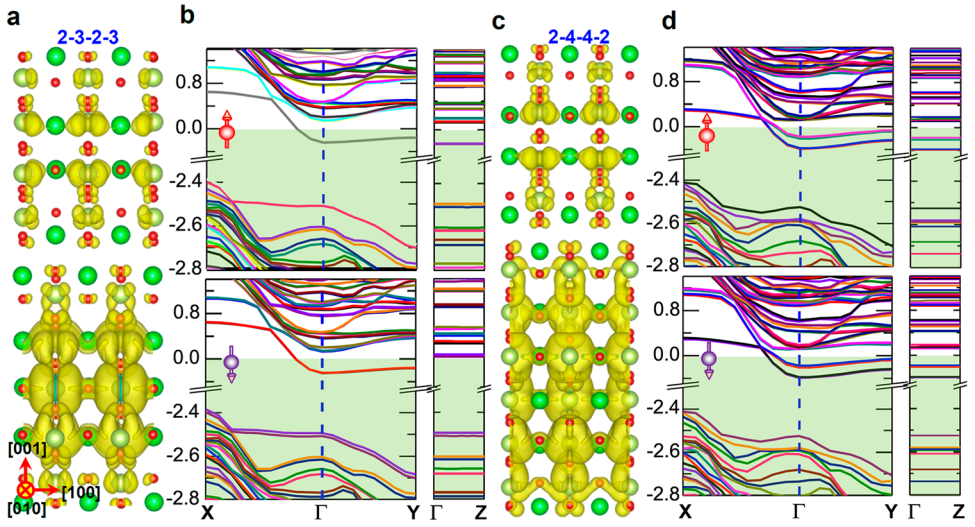

Figure 4. Charge density isosurface integrated in the energy window (E_F−0.5 eV, E_F) viewed along the *b* projection and band structure calculated along high-symmetry lines: (a, b) 2−3−2−3 and (c, d) 2−4−4−2. The charges are dominantly localized at the Nb cations in the chain-like slabs with a small degree of leakage to the zigzag-like slabs. The band structures of both structures reveal a quasi-1D dispersion for the degenerate conduction bands near E_F, which comprises a strong dispersion along the Γ−*X*, a relatively weak dispersion along Γ−*Y*, and no discernible dispersion along the Γ−*Z*. The E_F is set to zero.

among the HAADF STEM images is the thickness of the chain-like slabs which have uniform two atomic layers in Figure 1a (corresponding to $Sr_nNb_nO_{3n+2}$ with n = 4), uniform three atomic layers in Figure 1b (n = 5), and alternately arranged two and three atomic layers in Figure 1c (n = 4 and 5), respectively. Figure 1d shows a structure comprising chain-like slabs with two and four atomic layers (n = 4 and 6), which has so far been fabricated only by the electron irradiation of the $SrNbO_{3.4}$ (n = 5) structure with a proper dose rate.[21] The transport data of the 2−4−4−2 structure are now still unavailable from direct electrical measurements. In light of these structural characteristics of the chain-like slabs, these four compounds are named as 2−2−2−2, 3−3−3−3, 2−3−2−3, and 2−4−4−2, respectively.

To probe the valence states of the Nb cations in the $Sr_nNb_nO_{3n+2}$ compounds, we have conducted electron energy-loss spectroscopy (EELS) measurements of the O−K edges (Figure 2) taken from the chain-like and the zigzag-like slabs. From the results it is possible to obtain the valence state of Nb and evaluate the electrical properties of corresponding local structures.[22,23] As shown in Figure 2, the O−K edges are characterized mainly by two edge onsets (denoted *a* and *b* peaks). Since the Nb atoms in the $Sr_nNb_nO_{3n+2}$ compounds are octahedrally surrounded by O atoms, the Nb 4d orbitals will split into the upper e_g and lower t_{2g} orbitals. The *a* and *b* peaks can be approximately identified as the t_{2g} and e_g components of the Nb 4d-O 2p orbital overlapping, respectively. The t_{2g} and e_g orbitals can accept six and four electrons, respectively. The ratio of empty orbits e_g/t_{2g} for Nb^{5+} is 4/6, while that for Nb^{4+} is 4/5. In a very simplified explanation, the peak intensity ratio b/a should qualitatively reflect the Nb valence state: The intensity ratio b/a for Nb^{4+} will be obviously larger than that for Nb^{5+}. The two peaks from the zigzag-like slabs in all the $Sr_nNb_nO_{3n+2}$ compounds (labeled by B, C, F, and I) have a similar height with height ratios b/a smaller than 1.2. This suggests that the Nb cations in the zigzag-like slabs have a valence state of +5, inducing an insulating nature in these regions. The *b* peaks from the three-layer and four-layer thick chain-like slabs (labeled by D, G, and J) are significantly higher than the *a* peaks. The height ratios b/a are near 1.5. This result suggests that the Nb cations in these slabs have a valence state of +4, resulting in a metallic conductivity in these regions. Interestingly, the O−K edges from the two-layer thick chain-like slabs in the 2−3−2−3 and 2−4−4−2 structures (labeled by E and H, respectively) are completely different from those in the 2−2−2−2 structure (labeled by A). As can be seen, the *b* peaks from the E and H slabs are much higher than the *a* peaks (b/a larger than 1.35, close to the three-layer thick slabs), while the *a* and *b* peaks from the A slab have a b/a ratio of 1.22, similar as the ratios in the zigzag slabs. This suggests that the two-layer thick chain-like slab changes from insulating in the 2−2−2−2 structure to conducting in the 2−3−2−3 and 2−4−4−2 structures. Obviously, the EELS results reveal a 3D insulting nature in the 2−2−2−2 structure and a highly anisotropic electrical conductivity in the 3−3−3−3, 2−3−2−3, and 2−4−4−2 structures which exhibit the highest conductivity within the chain-like slabs, showing a quasi-2D characteristics.

To gain more insight into the physical mechanism underlying the valence states variations and into the quantum nature of confined charges, we carried out density functional theory (DFT) calculations using a generalized gradient approximation (GGA) on the fully relaxed structures. Figure 3 gives the optimized structural models, the total density of states (TDOS) and the layer-resolved Nb-4d projected density of states (PDOS) of the $Sr_nNb_nO_{3n+2}$ compounds. The simulated HAADF images (Supplementary Figure S2) using the optimized structure models are consistent with the experimental ones, suggesting a correct model construction and structural relaxation in the DFT calculations. The TDOS of the 2−2−2−2 type structure in Figure 3a uncovers its intrinsic insulating nature. On the contrary, the 3−3−3−3 type structure is conducting due to the emergence of states at Fermi-level (E_F) which mainly comes from Nb-d electrons (Figure 3b). The corresponding PDOS further reveals that the states at E_F originate mainly from the Nb-d electrons from the chain-like slabs rather than the zigzag-like slabs, suggesting a strong anisotropy in the electrical nature of the 3−3−3−3 type structure. For example, the Nb4 cation in the chain-like slab

DOI: 10.1021/acsnano.7b06619
ACS Nano 2017, 11, 12519−12525

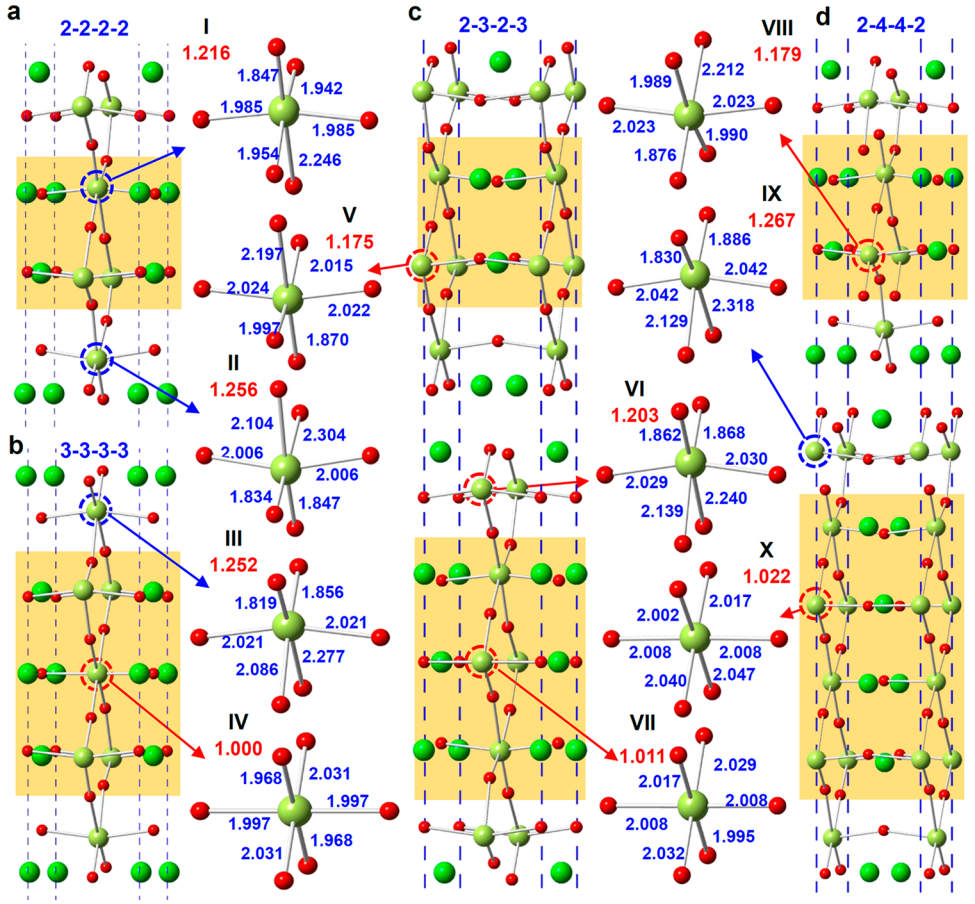

Figure 5. Representative NbO_6 octahedra extracted from the chain-like and zigzag-like slabs and the bond length of the three pairs of Nb−O bonds. (a) 2−2−2−2, (b) 3−3−3−3, (c) 2−3−2−3, and (d) 2−4−4−2. The chain-like slabs are highlighted by yellow shading. All NbO_6 octahedra (*i.e.*, II, III, VI, and IX) from the zigzag-like slabs have larger Nb−O bond length ratios compared to those from the chain-like slabs, indicating a larger displacement of Nb cations from the octahedral centers.

donates significantly more electrons compared to the Nb3 cation in the zigzag slab. The decomposed PDOS in Supplementary Figure S3 suggests that the Nb4-d states originate mainly from the d_{xy} and d_{xz} orbitals. The TDOS results also indicate that the 2−3−2−3 type structure is conducting (Figure 3c). As expected, the PDOS from the zigzag-like slab (*i.e.*, Nb6-d) and that from the three-layer thick chain-like slab (*i.e.*, Nb7-d) are extremely similar to their counterparts in the 3−3−3−3 type structure (*i.e.*, Nb3-d and Nb4-d). The Nb7-d orbital which is mainly composed of the d_{xy} and d_{xz} orbitals (Supplementary Figure S4), accumulates more electrons at E_F than the Nb6-d orbital. Interestingly, in contrast to the intrinsic insulating nature of the 2−2−2−2 type structure, the two-layer thick chain-like slab in the 2−3−2−3 type structure becomes conducting due to the slight but visible emergence of d_{xy} states at E_F, as clearly represented by the PDOS and decomposed PDOS of Nb5-d in Figure 3d and Supplementary Figure S4. Similarly, the DOS results in Figure 3d and Supplementary Figure S5 reveal that the 2−4−4−2 type structure comprises conducting two-layer and four-layer thick chain-like slabs (*i.e.*, Nb8-d and Nb10-d) and in between insulating zigzag slabs (*i.e.*, Nb9-d), exhibiting a quasi-1D metallic conducting feature. The 4−4−4−4 type structure, if fabricated successfully, should also be a quasi-1D metallic conductor (Supplementary Figure S6). To further check the effects of the localization of Nb-4d electrons, we performed GGA+U calculations in Dudarev's approach, and the results (*i.e.*, Supplementary Figure S7) validate the standard DFT-GGA calculations. Therefore, the DOS results unambiguously indicate that the 3−3−3−3, 2−3−2−3, and 2−4−4−2 type structures are quasi-1D metallic conductors and the 2−2−2−2 type structure is a 3D insulator, which is consistent with the EELS measurements.

To shed more light on the quantum confinement and the 2D conductivity inside the compounds, we further computed the partial charge density close to E_F and band structures of the 2−3−2−3 and 2−4−4−2 type structures. Figure 4a shows an electron density isosurface for the electronic states near E_F of the 2−3−2−3 type structure. The electrons are dominantly localized at the Nb cations in the three-layer and two-layer thick chain-like slabs with a small degree of leakage to the zigzag-like regions, indicating an anisotropic electrical conductivity. The band structure in Figure 4b reveals a quasi-1D dispersion for the degenerate conduction bands near E_F, which comprises a strong dispersion along the $\Gamma-X$ (*i.e.*, the *a* axis in real space), a relatively weak dispersion along $\Gamma-Y$ (*i.e.*, the *b* axis in real space), and no discernible dispersion along the $\Gamma-Z$ (*i.e.*, the *c* axis in real space). This means the 2−3−2−3 type structure is a quasi-1D conductor with the highest conductivity along the *a* axis. The charge distribution (Figure 4c) and the band structure (Figure 4d) of the 2−4−4−2 structure share many similarities with those of the 2−3−2−3 type structure, indicating a quasi-1D conducting nature in this compound. The results are consistent with the PDOS analysis.

DOI: 10.1021/acsnano.7b06619
ACS Nano 2017, 11, 12519−12525

Since electrons at E_F surround mainly the Nb and O ions, the local atomic structure of the NbO_6 octahedra should be a major factor determining the electrical properties of the $Sr_nNb_nO_{3n+2}$ compounds. Thus, we systematically examine the configuration of the NbO_6 octahedra to reveal the underlying mechanism for the quasi-1D electrical properties of the $Sr_nNb_nO_{3n+2}$ compounds. Figure 5 presents the representative NbO_6 octahedra (named I–X) extracted from the chain-like slabs (highlighted by yellow shading) and the zigzag-like slabs and the bond length of the three pairs of Nb–O bonds. The bond length ratios of each pair in opposite directions were calculated, and the largest ratio among the three pairs was presented to define the displacement of Nb from the octahedral center. Interestingly, all NbO_6 octahedra (*i.e.*, II, III, VI, and IX) from the zigzag-like slabs have the largest Nb–O bond length ratio exceeding 1.2, indicating a severe displacement of Nb from the octahedral centers. However, all NbO_6 octahedra (*i.e.*, IV, VII and X) from the three-layer thick chain-like slabs of the 2–3–2–3 and 3–3–3–3 type structures and the four-layer thick chain-like slabs in the 2–4–4–2 type structure have bond length ratios near 1.0, indicating a nearly undistorted shape of these octahedra with almost no displacement of Nb cations from the octahedral centers. It is worth noting that the NbO_6 octahedra V and VIII from the two-layer thick chain-like slabs in the 2–3–2–3 and 2–4–4–2 type structures have the highest bond length ratios, namely about 1.17, which is obviously smaller than that of the 2–2–2–2 structure, namely 1.216, rendering their electrical properties completely different. To further confirm the direct correlation between the electrical properties and the shape of the NbO_6 octahedra, we conducted a crude test by using the insulating 2–2–2–2 structure. As shown in Supplementary Figure S8, states emerge at E_F if the two octahedra (*i.e.*, Nb1′-O_6 and Nb2′-O_6) in the chain-like slab are deliberately modified through moving the displaced Nb cations toward the centers of the NbO_6 octahedra, thereby inducing a conducting nature in this structure.

CONCLUSIONS

In summary, we have demonstrated that the perovskite-related $Sr_nNb_nO_{3n+2}$ compounds with 2–3–2–3, 3–3–3–3, and 2–4–4–2 type structures are quasi-1D metallic conductors, while the 2–2–2–2 type structure exhibits an insulating nature. The zigzag-like slabs in all these structures as well as the chain-like slabs in the 2–2–2–2 type structure are electrically insulating because the NbO_6 octahedra in these slabs are significantly distorted with a large displacement of Nb from the octahedral centers and the Nb valence is Nb^{5+}. The chain-like slabs in the 2–3–2–3, 3–3–3–3, and 2–4–4–2 type structures are conducting since their Nb valence/electron configuration is $Nb^{(5-w)+}/4d^w$ with $w > 0$. The nearly undistorted NbO_6 octahedra lead to a metallic conductivity along the *a*-axis. The $Sr_nNb_nO_{3n+2}$ quasi-1D conductors are composed of alternately stacked chain-like conducting slabs and zigzag-like insulating slabs, which can be derived by intercalating the insulating zigzag-like slabs into the 3D conducting $SrNbO_3$ perovskite along {110} planes. Such a concept of segmenting a 3D conductor into a stack of quasi-2D conducting thin layers by inserting insulating layers in between them should be applicable not only to $SrNbO_3/SrNbO_{3+y} = Sr_nNb_nO_{3n+2}$ but also to other materials. This may find applications in the development of 2D electrical conducting materials and devices.

METHODS

Sample Preparation and Microscopic Observation. The $Sr_nNb_nO_{3n+2}$ compounds $SrNbO_{3.4}$ (n = 5), $SrNbO_{3.45}$ (n = 4.5), and $SrNbO_{3.5}$ (n = 4) in crystalline form were grown by floating zone melting under an argon, argon plus hydrogen, and air atmosphere, respectively.[8,9,20] The oxygen content of the crystalline samples was determined by thermogravimetric analysis.[8,20] Thin-foil specimens for STEM imaging were prepared by cutting and grinding the crystal slices down to 20 μm. An Ar ion-beam thinning process using an accelerating gun voltage of 1–4 kV and an incident beam angle of 4–5° was subsequently applied. HAADF STEM observations were performed using a 200 kV STEM (ARM200FC, JEOL) equipped with a probe corrector (CEOS GmbH) which offers an unprecedented opportunity to probe structures with sub-angström resolution. For the HAADF STEM imaging a probe size of <1 Å, a probe convergence angle of ~25 mrad and a collection semiangle of 68–280 mrad were used. The STEM is equipped with a Gatan Enfina system which was used to record EELS spectra with an energy resolution (full-width half-maximum) of ~0.5 eV.

DFT Calculations. DFT calculations were performed using the projector augmented wave (PAW) method[24] as implemented within Vienna *ab Initio* Simulation Package (VASP).[25,26] The generalized gradient approximation (GGA) within the Perdew and Wang (PW91) scheme[27] was employed to describe the exchange–correlation functional. The valence-electron wave functions were expanded in a plane wave basis with energies up to 400 eV, and an 8 × 6 × 2 Monkhorst–Pack *k*-point grid was employed in the supercell calculations. The tetrahedron method with Blöchl correction was used for the self-consistent calculation. All of the atoms in the system were fully relaxed with the conjugate gradient (CG) algorithm until the magnitude of the Hellmann–Feynman force on each atom converged to <0.05 eV/Å. We adopted the rotationally invariant DFT +U formulation of Dudarev[28] and the effective Hubbard parameter ($U_{eff} = U - J$) (U = 8.8 eV, J = 1.0 eV)[29] to consider the effect of the localization of Nb-4d electrons. The reproduced band gap of $Sr_2Nb_2O_7$ is 3.758 eV, which agrees well with the experimental value (3.9 eV).[30]

ASSOCIATED CONTENT

Supporting Information

The Supporting Information is available free of charge on the ACS Publications website at DOI: 10.1021/acsnano.7b06619.

Characterizations: HAADF and DPC STEM images; Simulated HAADF and ABF images. Chemical identification: electron energy-loss spectroscopy. Theoretical calculations: atomic models; DOS (PDF)

AUTHOR INFORMATION

Corresponding Authors

*E-mail: clchen@imr.ac.cn.
*E-mail: xlma@imr.ac.cn.
*E-mail: ikuhara@sigma.t.u-tokyo.ac.jp.

ORCID

Chunlin Chen: 0000-0003-1985-1940

Notes

The authors declare no competing financial interest.

ACKNOWLEDGMENTS

C.C. thanks support from the Key Research Program of Frontier Sciences, CAS (no. QYZDY-SSW-JSC027), "Thousand Youth Talents Plan" of China and Prof. Hengqiang Ye in Institute of Metal Research, CAS. C.C. and Y. I. acknowledge the support by Grant-in-Aid for Specially Promoted Research (Grant No. JP17H06094 from JSPS, and "Nanotechnology Platform" (Project No. 12024046) of MEXT. F.L. thanks Nicola Spaldin for her support.

DOI: 10.1021/acsnano.7b06619
ACS Nano 2017, 11, 12519–12525

REFERENCES

(1) Mannhart, J.; Schlom, D. G. Oxide Interfaces-An Opportunity for Electronics. *Science* **2010**, *327*, 1607−1611.

(2) Chambers, S. A. Epitaxial Growth and Properties of Doped Transition Metal and Complex Oxide Films. *Adv. Mater.* **2010**, *22*, 219−248.

(3) Okamoto, S.; Millis, A. J. Electronic Reconstruction at an Interface between a Mott Insulator and a Band Insulator. *Nature* **2004**, *428*, 630−633.

(4) Ohtomo, A.; Hwang, H. Y. A High-Mobility Electron Gas at the $LaAlO_3/SrTiO_3$ Heterointerface. *Nature* **2004**, *427*, 423−426.

(5) Thiel, S.; Hammerl, G.; Schmeh, A.; Schneider, C. W.; Mannhart, J. Tunable Quasi-Two-Dimensional Electron Gases in Oxide Heterostructures. *Science* **2006**, *313*, 1942−1945.

(6) Jang, H. W.; Felker, D. A.; Bark, C. W.; Wang, Y.; Niranjan, M. K.; Nelson, C. T.; Zhang, Y.; Su, D.; Folkman, C. M.; Baek, S. H.; Lee, S.; Janicka, K.; Zhu, Y.; Pan, X. Q.; Fong, D. D.; Tsymbal, E. Y.; Rzchowski, M. S.; Eom, C. B. Metallic and Insulating Oxide Interfaces Controlled by Electronic Correlations. *Science* **2011**, *331*, 886−889.

(7) Verissimo-Alves, M.; García-Fernández, P.; Bilc, D. I.; Ghosez, P.; Junquera, J. Highly Confined Spin-Polarized Two-Dimensional Electron Gas in $SrTiO_3/SrRuO_3$ Superlattices. *Phys. Rev. Lett.* **2012**, *108*, 107003.

(8) Lichtenberg, F.; Herrnberger, A.; Wiedenmann, K.; Mannhart, J. Synthesis of Perovskite-Related Layered $A_nB_nO_{3n+2}$ = ABO_X Type Niobates and Titanates and Study of Their Structural, Electric and Magnetic Properties. *Prog. Solid State Chem.* **2001**, *29*, 1−70.

(9) Lichtenberg, F.; Herrnberger, A.; Wiedenmann, K. Synthesis, Structural, Magnetic and Transport Properties of Perovskite-Related Layered Titanates, Niobates and Tantalates of the Type $A_nB_nO_{3n+2}$, $A'A_{k-1}B_kO_{3k+1}$ and $A_mB_{m-1}O_{3m}$. *Prog. Solid State Chem.* **2008**, *36*, 253−387.

(10) Isawa, K.; Itti, R.; Sugiyama, J.; Koshizuka, N.; Yamauchi, H. Synthesis and Transport Properties of Sr_xNbO_3 ($0.75 \leq x \leq 0.90$). *Phys. Rev. B: Condens. Matter Mater. Phys.* **1994**, *49*, 3534.

(11) Chen, C. L.; Lv, S.; Wang, Z.; Akagi, K.; Lichtenberg, F.; Ikuhara, Y.; Bednorz, J. G. Atomic and Electronic Structure of the $SrNbO_3/SrNbO_{3.4}$ Interface. *Appl. Phys. Lett.* **2014**, *105*, 221602.

(12) Kuntscher, C. A.; Schuppler, S.; Haas, P.; Gorshunov, B.; Dressel, M.; Grioni, M.; Lichtenberg, F.; Herrnberger, A.; Mayr, F.; Mannhart, J. Extremely Small Energy Gap in the Quasi-One-Dimensional Conducting Chain Compound $SrNbO_{3.41}$. *Phys. Rev. Lett.* **2002**, *89*, 236403.

(13) Kuntscher, C. A.; Schuppler, S.; Haas, P.; Gorshunov, B.; Dressel, M.; Grioni, M.; Lichtenberg, F. Electronic and Vibrational Properties of Low-Dimensional Perovskites $Sr_{1-y}La_yNbO_{3.5-x}$. *Phys. Rev. B: Condens. Matter Mater. Phys.* **2004**, *70*, 245123.

(14) Kuntscher, C. A.; Gerhold, S.; Nücker, N.; Cummins, T. R.; Lu, D. H.; Schuppler, S.; Gopinath, C. S.; Lichtenberg, F.; Mannhart, J.; Bohnen, K.-P. Electronic Structure of Layered Perovskite-Related $Sr_{1-y}La_yNbO_{3.5-x}$. *Phys. Rev. B: Condens. Matter Mater. Phys.* **2000**, *61*, 1876−1883.

(15) Weber, J.-E.; Kegler, C.; Buttgen, N.; Krug von Nidda, H.-A.; Loidl, A.; Lichtenberg, F. NMR, EPR, and Bulk Susceptibility Measurements of One-Dimensional $SrNbO_{3.41}$. *Phys. Rev. B: Condens. Matter Mater. Phys.* **2001**, *64*, 235414.

(16) de Campos, A.; da Luz, M. S.; dos Santos, C. A. M.; Rice, A. T.; Deml, A. M.; White, B. D.; Neumeier, J. J.; Cohn, J. L. Physical Properties of Quasi-One-Dimensional $SrNbO_{3.41}$ and Luttinger Liquid Analysis of Electrical Transport. *Phys. Rev. B: Condens. Matter Mater. Phys.* **2010**, *82*, 125117.

(17) Kobayashi, W.; Hayashi, Y.; Matsushita, M.; Yamamoto, Y.; Terasaki, I.; Nakao, A.; Nakao, H.; Murakami, Y.; Moritomo, Y.; Yamauchi, H.; Karppinen, M. Anisotropic Thermoelectric Properties Associated with Dimensional Crossover in Quasi-One-Dimensional $SrNbO_{3.4+d}$ ($d \sim 0.03$). *Phys. Rev. B: Condens. Matter Mater. Phys.* **2011**, *84*, 085118.

(18) Nanamatsu, S.; Kimura, M.; Kawamura, T. Ferroelectric Properties of $Sr_2Nb_2O_7$ Single Crystal. *J. Phys. Soc. Jpn.* **1975**, *38*, 817−824.

(19) Atuchin, V. V.; Grivel, J.-G.; Korotkov, A. S.; Zhang, Z. Electronic Parameters of $Sr_2Nb_2O_7$ and Chemical Bonding. *J. Solid State Chem.* **2008**, *181*, 1285−1291.

(20) Lichtenberg, F.; Williams, T.; Reller, A.; Widmer, D.; Bednorz, J. G. Electric and Magnetic Properties of the First Layered Conducting Titanium and Niobium Oxides. *Z. Phys. B: Condens. Matter* **1991**, *84*, 369−374.

(21) Chen, C. L.; Wang, Z.; Lichtenberg, F.; Ikuhara, Y.; Bednorz, J. G. Patterning Oxide Nanopillars at the Atomic Scale by Phase Transformation. *Nano Lett.* **2015**, *15*, 6469−6474.

(22) Bach, D.; Schneider, R.; Gerthsen, D.; Verbeeck, J.; Sigle, W. EELS of Niobium and Stoichiometric Niobium-Oxide Phases-Part I: Plasmon and Near-Edges Fine Structure. *Microsc. Microanal.* **2009**, *15*, 505−523.

(23) Bach, D.; Schneider, R.; Gerthsen, D. EELS of Niobium and Stoichiometric Niobium-Oxide Phases-Part II: Quantification. *Microsc. Microanal.* **2009**, *15*, 524−538.

(24) Blöchl, P. E. Projector Augmented-Wave Method. *Phys. Rev. B: Condens. Matter Mater. Phys.* **1994**, *50*, 17953−17979.

(25) Kresse, G.; Furthmüller, J. Efficient Iterative Schemes for *Ab Initio* Total-Energy Calculations using a Plane-Wave Basis Set. *Phys. Rev. B: Condens. Matter Mater. Phys.* **1996**, *54*, 11169−11186.

(26) Kresse, G.; Furthmüller, J. Efficiency of *Ab-Initio* Total Energy Calculations for Metals and Semiconductors using a Plane-Wave Basis Set. *Comput. Mater. Sci.* **1996**, *6*, 15−50.

(27) Perdew, J. P.; Chevary, J. A.; Vosko, S. H.; Jackson, K. A.; Pederson, M. R.; Singh, D. J.; Fiolhais, C. Atoms, Molecules, Solids, and Surfaces - Application of the Generalized Gradient Approximation for Exchange and Correlation. *Phys. Rev. B: Condens. Matter Mater. Phys.* **1992**, *46*, 6671.

(28) Dudarev, S. L.; Botton, G. A.; Savrasov, S. Y.; Humphreys, C. J.; Sutton, A. P. Electron-Energy-Loss Spectra and the Structural Stability of Nickel Oxide: An LSD+U Study. *Phys. Rev. B: Condens. Matter Mater. Phys.* **1998**, *57*, 1505−1509.

(29) Meng, Q.; Wang, T.; Liu, E.; Ma, X.; Ge, Q.; Gong, J. Understanding Electronic and Optical Properties of Anatase TiO_2 Photocatalysts Co-Doped with Nitrogen and Transition Metals. *Phys. Chem. Chem. Phys.* **2013**, *15*, 9549−9561.

(30) Kudo, A.; Kato, H.; Nakagawa, S. Water Splitting into H_2 and O_2 on New $Sr_2M_2O_7$ (M= Nb and Ta) Photocatalysts with Layer Perovskite Structures: Factors Affecting the Photocatalytic Activity. *J. Phys. Chem. B* **2000**, *104*, 571−575.

DOI: 10.1021/acsnano.7b06619
ACS Nano 2017, 11, 12519−12525